Effect of cross channel salinity imbalance due to freshwater influence in a narrow estuary

Senior Thesis

31 May 2015

Robert J. Daniels

University of Washington

School of Oceanography

1503 NE Boat Street

Seattle, Washington 98105

rdan15@uw.edu

Acknowledgements

This Study was funded by the University of Washington and its School of Oceanography. I thank the entire 2015 senior thesis class, student and faculty, for their assistance with data collection, help with analysis, and advisement during the course of this project. I especially thank Charles Eriksen for providing excellent and patient guidance throughout the duration of the study. I would also like to thank Arthur Nowell for providing reviews and useful comments on pre-cruise preparation paperwork and the subsequent study's paper.

Abstract

Nootka Sound is a group of narrow and deep fjord-like inlets on the west coast of Vancouver Island. This understudied estuarine system was the focus of an 11 December to 21 December 2014 University of Washington's School of Oceanography Senior Cruise, in part, looking for insights in to questions of cross channel density structure effects on circulation in narrow basins. In particular, the study looked at the contributions of high freshwater input, a ubiquitous condition from heavy rains during the winter months in this area, and its effect on the transverse density structure. We examined the zonal density imbalance that could lead to the development of geostrophic currents in river fed sub-basins during the season of highest precipitation.

Introduction

The breadth of past research in estuaries almost exclusively focused on longitudinal and vertical processes, owing to the paramount importance of along channel transport of salt and other materials when dealing with estuary processes (Dyer 1997; Farmer et al. 1983). Researchers tend to largely neglect the important contribution of lateral dynamics to the system, especially with narrow basins where geostrophic currents and thermal wind, the product of cross-channel balance of a horizontal pressure gradient and Coriolis effect (Cameron 1951, Gill 1982) are understudied phenomenon. On average, the basins of Nootka Sound have in common with all fjordal systems a small river discharge when compared to the total fjord volume and substantial stratification that is confined to relatively thin layer near the surface (Dyer 1997). Yet a persistent significantly large freshwater input, as found during the heavy rain winter months, can allow a basin to adjust in to a state of geostrophic equilibrium, thus making geostrophic currents a potential component of the overall water column velocity.

The investigation was motivated by a study conducted by Cameron (1951), who found a persistent transverse salinity imbalance at the mouth of Portland inlet in Chatham Sound on the Northwest coast of British Columbia, which he hypothesized could create an approximate balance between Coriolis force and the transverse pressure gradient. He attributed this cross channel variability to high river run-off from the Nass and Skeena Rivers. Higher concentrations of fresher water were observed on the right side of the basin, when looking from the inlet's head, with an approximate 3 PSU difference across channel down to 60 meters, which Cameron established as the surface of no motion. Cameron points out that in most estuaries, foregoing simplifying assumptions may not be applicable due to the large frictional effects of bottom and lateral boundaries and accelerations and frictional effects of associated mixing of fresher estuary

water and sea water. He proposed that the inlets along the coast of British Columbia represented an estuary type where these complicating factors are suppressed due to the fjords long, narrow, and deep characteristics, with plunging side-walls and average basin depths of over 100 meters. Portland Inlet is a comparable width and depth with that of Muchalat and Tahsis Inlets of Nootka Sound, justifying ignoring frictional and mixing components that may hamper the development of geostrophy.

Further impetus for the study was a Bute Inlet study performed by Tabata and Pickard (1957). Bute Inlet, a mainland analogue of Nootka Sound, was observed having a strong cross-inlet density gradient attributable to a western boundary riverine sourced fresh water flux. Data presented by Tabata and Pickard (1957) exposed a transverse salinity imbalance of approximately 5.0 PSU between fresher surface salinity on the right side of the basin, when looking from the fjord head, and the higher salinity left side during a period of high runoff, which were due to glacial melt during summer months. Similar climatic forcing tends to exist in the sub-basins of Nootka Sound during the months of November and December, which is the period of largest annual rain fall. Tahsis River had a December 1998 mean discharge of 15305 L s^{-1} compared to the annual mean of 8348 L s^{-1} and Gold River had a December 1998 mean discharge of 133840 L s^{-1} compared to the annual mean of 83000 L s^{-1} (Jackson and Cook 1999). These mean discharges are representative of the average November and December mean discharges.

This study was performed with the working hypothesis that the lateral basin dynamics will reflect density imbalance conditions with inflow of more saline water on the southern side and outflow of fresher water on the northern side of Muchalat inlet and inflow of more saline water on the eastern side and outflow of fresher water on the west side of Tahsis inlet, similar to

what was observed by Cameron (1951). Rapid data collection facilitated by use of a recent technological advance, the UnderwayCTD (UCTD), allowed for high resolution sections and greatly reduce the possible effects of temporal variability on data sets (Forrester 1970) by considerably reducing the time it took to complete a section. The positive result of the study establishes the importance of considering the cross-channel components when deliberating the contributions of current in narrow estuarine channels with high freshwater flux. The study examines the need to move beyond the present assumptions that longitudinal currents in narrow inlets are driven exclusively by an along-channel density gradient. Transverse gradient and forcing from the earth's rotation may play a very important role in narrow estuarine circulation.

Methods

Surveys were conducted using the UCTD; a Seabird CTD equipped, quick deployment and recovery package, with Bluetooth wireless communication, a "gravity pumped" conductivity cell, pressure, and temperature sensors all sampling at 16Hz (Teledyne Oceanscience. 2014). In both Muchalat and Tahsis Inlet, a "tow-yo" like UCTD operation was employed across the basins. Transects were performed at 2 knots which allowed for an average of 7 casts per section. Water column velocity measurements were collected using the ship's hull-mounted ADCP and the CODAS ADCP processing software to bin and average the data for analysis.

The surveys conducted in Muchalat and Tahsis looked at the density structure by collecting temperature (ºC), salinity (PSU), and pressure (p) measurements from the UCTD. The two basins were chosen due to the large rivers at their heads and their relatively unobstructed, straight channels. The Tahsis sections were performed across the north portion of the basin, starting with station Tu1 south of the Leiner River, proceeding southward to Tu6 north of

Tsowwin River (Fig. 1). The Muchalat survey was operated across the Eastern end of the basin, starting at Mu1, at the mouth of the Gold River and heading westward to Mu3 to approximately 1 km west of Victor Island (Fig. 2). Muchalat, which has an approximately maximum depth of 320 meters, and Tahsis, which has an approximately maximum depth of 200 meters, had a similar across channel sampling time of approximately 40 minutes.

Resulting horizontal pressure gradients and their calculated geostrophic currents have been averaged and normalized, conserving for the mass of inflows and outflows in two dimensions. A right-handed coordinate system has been adopted for which $v(y)$ is the along-fjord velocities and $u(x)$ is the across-fjord velocities. Along-fjord components of velocity(v) will be positive up fjord (toward the head of the basin).

Temperature, salinity, and calculated density data collected by the UCTD were averaged into one meter bins, after which anomalous data was corrected by coefficients derived from averaging surrounding data points. A first degree linear fit was calculated for each bin depth in a cross channel section, providing an averaged across channel density slope $\frac{\partial \rho}{\partial x}$. The steady state equations in linearized form was used to solve for vertical shear, $\frac{\partial v}{\partial z}$ up the water column at each depth using the calculated density slope

$$-fv = -\frac{1}{\rho_o}\frac{\partial p}{\partial x},$$

$$fu = -\frac{1}{\rho_o}\frac{\partial p}{\partial y},$$

$$\frac{\partial p}{\partial z} = -\rho g\ ,$$

where f is the local Coriolis parameter, ρ_o is the reference density, g is local acceleration of gravity. $\frac{\partial \rho}{\partial x}$ was the calculated density slope for each binned depth to calculate vertical shear

$$\frac{\partial v}{\partial z} = \frac{-g}{\rho_0 f}\frac{\partial \rho}{\partial z}$$

The product of the equation was then integrated up the water column,

$$V = \int_{-z}^{0} dv\, dz\,,$$

and adjusted along the x axis with consideration to adhering to the principal of conservation of mass, developing a profile of the entire water columns geostrophic velocities.

Results

This section presents the across-fjord density distributions assembled from transverse UCTD runs in Muchalat and Tahsis Inlets. As density is primarily controlled by salinity in a fjord-like estuary and salinity and density plots display very similar water column properties structures in fjords, density has been used in all figures. These across channel contour plots are included to help explain the proposed density driven along channel currents. The results section has been separated into two parts: the survey in Tahsis Inlet which will be presented first, followed by the results of the Muchalat Inlet survey. Both the inferred geostrophic currents and the mean ADCP data will be offered for each section.

Tahsis Inlet

All contour plots for Tahsis Inlet are oriented in a west to east direction. The mean calculated v-velocity in the north portion of Tahsis Inlet to Tahsis Narrows suggests a two

layered estuarine circulation. The observed physical properties of these cross-channel sections reveal a fresher top layer sits on the west side of the basin. This is an expected product of rotational forcing in the northern hemisphere, with fresh more buoyant outflow water forced to the right side of the basin and the saltier inflow forced to the left, when looking down channel from the head.

Sections Tu1, Tu2, and Tu3 were all preformed in succession (Fig. 3) during an ebbing tide. Tu1 (Fig. 4a.) had an integrated average geostrophic (IAG) inflow velocity at the surface of ~0.1877 m s^{-1} up from to 45 m and a ~-0.1840 m s^{-1} deeper outflow (Fig. 4b.). Section Tu2 (Fig. 5a) appears to have a reverse in current with a IAG surface outflow of ~-0.2118 m s^{-1} up from approximately 45 m (Fig. 5b.) where the current becomes predominately a weaker deep IAG inflow of ~0.1231 m s^{-1}. These high surface velocities significantly weakens and circulation retains its two layer structure at Tu3 (Fig. 6a), with an IAG velocity of ~0.0746 m s^{-1} surface inflow and a ~-0.0534 m s^{-1}deep outflow (Fig. 6b).

The mean ADCP velocities for these three sections that have been averaged across the basin in 8 m bins. They reveal very small velocities, fluctuating around 0 m s^{-1}.

At Tu4 (Fig. 7a.), south of Tahsis Narrows, there is still a distinct and large fresh water signal in the surface layers of the west side of the basin but the transverse horizontal pressure gradient is opposite of the former sections in the north. This opposes to what is expected from the hydrostatic forcing caused by the large fresh water body on the right side of the channel. The water column develops a more robust two layer circulation structure, with the inflow and outflow in the same direction as Tu3. This may be due to being run at the slack tide after the flood. A strong surface inflow, up from to 20 m, has an IAG velocity of ~0.5864 m s^{-1}. Below 20 m, there

is an IAG outflow of ~-0.1088 m s^{-1} from the bottom of the basin (Fig. 7b.). An anomalous 12 ° C water mass appears between 34 and 40 m on the west side of the basin. Isopycnals above this relatively warm water mass appear pushed up for the 100 m distance across the channel's length (Fig. 8). The mean ADCP shows slightly stronger velocities and more of a correlation between the trend of the calculated IAG velocities and observed ADCP velocities.

At Tu5 (Fig. 9a.), run at slack tide after the ebb, a distinct three layer circulation system become prominent, with reversed currents from Tu4. The surface outflow has a IAG velocity of ~-0.2392 m s^{-1} integrated up from 20 m, a mid-depth inflow with an IAG velocity of ~0.0920 m s^{-1} from between 55 to 20 m, and a deep IAG outflow with an average ~0.0053 m s^{-1} velocity (Fig. 9b.) below 55 m to the bottom. The anomalous warm water mass is not apparent in in this cross section. Again, the mean ADCP has weaker velocities that look to fit the trend and direction of IAG velocities.

Muchalat Inlet

All contour plots are oriented in a north to south direction. Muchalat Inlet's mean u-flow over the period of observation suggests a classic two-layer estuarine circulation structure. The characteristics of the basin's currents are higher velocity surface outflow and a slower deep inflow. A stronger freshwater signal is found on the north side of the basin, as would be expected due to the aforementioned rotational forcing on the fresh buoyant water mass.

Mu1 and Mu2 are characterized with a relatively stronger surface outflow to ~60 m and a region of weaker inflow at depth (Fig. 10a & Fig. 11a.). The vertical profiles of IAG

velocities reveal an averaged outflow, integrated to the surface from ~60 m depth was -0.0496 m s^{-1} (Fig. 10b) and a weaker inflow of 0.0159 m s^{-1} from the bottom to ~60 m at Mu1. At Mu2, a similar averaged integrated outflow to the surface from ~60 m depth of -0.0443 m s^{-1} and a weaker inflow of 0.0197 m s^{-1} (Fig. 11b.). Mean ADCP velocities up the water column are nearly 0 m s^{-1},but it's sign trend correlate well with the calculated geostrophic velocities. Both of these sections were run in succession at the end of an ebb tide.

Although the across-channel horizontal pressure gradient appears to be very slight,, the IAG velocities, increase downstream from the basin's head (Fig.12a.). Mu3 retains the two layer structure, with a stronger surface outflow, up from to ~60 m, averaged velocity of ~-0.2297 m s^{-1} (Fig. 12b.), with a weaker inflow of ~ 0.0705 m s^{-1} found below ~60 m to the bottom of the basin. The mean ADCP velocities was nearly 0 m s^{-1} up the water column.

Discussion

Fresh water input into the study's two basins almost certainly plays an important role in the inlets water column structure and overall circulation. Baroclinic conditions indeed exist in both Tahsis Inlet and Muchalat Inlet, though it is far more pronounced in the former. Tahsis has a smaller net river input, but the basin appears to be more effected by the fresh water flux. This may be due to the smaller overall width and/or the shallower depth of the Inlet, which could amplify the effects of fresh water forcing. It's very possible that the second and smaller fresh water source from the Tsowwin River contributes to this cross-channel horizontal pressure gradient; though an in-depth study tracing water properties would be needed to conclude this.

Calculated high velocities at the surface could not be verified using the bottom mounted ship-board ADCP due to the masking of the top 35.45 m of the raw data acquired by the ship-board system. Though the signs of v velocities can be interpreted as generally consistent with the signs of the calculated geostrophic v velocities in the majority of the sections, observed ADCP speeds are smaller than the calculated geostrophic velocities. There is overall agreement between the trends of the velocities taken from the ADCP and velocities derived from density calculations, adding validity to the proposed geostrophic and thermal wind driven currents. The smaller or inconsistent velocities could be the product of tidal forcing effecting the movement of the water column or passing Kelvin waves disrupting the flow of the water.

The reverse of the baroclinic condition found at Tu4 is hard to adequately address. The source of the anomalous 12 ° C water mass, a potential colperate, could be of open ocean origin, entering Tahsis Inlet through Tahsis Narrows. The sill at the mouth of Esperanza Inlet, west of the Tahsis Narrows, is a very shallow approximately 20 m sill which could inhibit deep water influx, allowing only occasional mid-depth oceanic water to enter the system. Such water would probably have a similar warm and dense signal that this water mass displays. Tu3 is devoid of a 12° C water mass signal, but Tu1 and Tu2 have strong mid-depth 12° to 12.2° C signal capped in by colder river sourced water and cold deep water. Whether this mid-depth water was disrupting the basin's salinity balance or if the reversal is due to tides or internal waves is an interesting question that will be left unanswered. Also, the query arises whether this is last summer's warm surface water or open ocean sourced water sequestered in the middle part of the basin?

When considering a similar survey in the future, one needs to contemplate its effects of tide on the final data set (Fig. 3). It was assumed that a single set of sections carried out successively in a basin would provide a substantial data set. This assumption relied on finding a more pronounced baroclinic condition in the fjord. A tidally averaged data set would be essential to ascertaining a truer picture of geostrophic currents, which would involve taking repeat cross-channel section at different phases of the tide, i.e. high, low, and slack tide. This would allow for the averaging out and elimination of the potentially large effects on the density structure due to tidal inflow and outflow. Owing to this problem, this data set does not allow for rigorous explanations of the effects of freshwater influences, general density structure due to salinity, and rotational effects in the estuary. This project was a step in the right direction, along with studies being published by researchers working in the Chilean fjords, who are asking similar questions in comparable environments,

Figure Captions

Fig. 1. Transverse UCTD stations along Tahsis Inlet, originating at Tu1 and terminating at Tu5. Blue lines indicate ship track in the survey area during the four day survey of the basin.

Fig. 2. Transverse UCTD stations along Muchalat Inlet, originating at Mu1 and terminating at Mu3. Blue lines indicate ship track in the survey area during the three day survey of the basin.

Fig. 3. Tide at Gold River at the head of Muchalat Inlet. Blue line is the estimated tide and red line is the tidal derivative representing estimated current.

Fig. 4. a) West to east contour plot of density in Tahsis Inlet from UCTD transect Tu1. Density is reported in sigma theta. b) Calculated geostrophic velocities and mean ADCP velocities against depth for cross-channel UCTD transect Tu1. Velocities are reported in m s^{-1}, with positive velocities as along-channel inflows and negative velocities as along-channel outflows.

Fig. 5. a) West to east contour plot of density in Tahsis Inlet from UCTD transect Tu2. Density is reported in sigma theta. b) Calculated geostrophic velocities and mean ADCP velocities against depth for cross-channel UCTD transect Tu2. Velocities are reported in m s^{-1}, with positive velocities as along-channel inflows and negative velocities as along-channel outflows.

Fig. 6. a) West to east contour plot of density in Tahsis Inlet from UCTD transect Tu3. Density is reported in sigma theta. b) Calculated geostrophic velocities and mean ADCP velocities against depth for cross-channel UCTD transect Tu3. Velocities are reported in m s^{-1}, with positive velocities as along-channel inflows and negative velocities as along-channel outflows.

Fig. 7. a) West to east contour plot of density in Tahsis Inlet from UCTD transect Tu4. Density is reported in sigma theta. b) Calculated geostrophic velocities and mean ADCP velocities against

depth for cross-channel UCTD transect Tu4. Velocities are reported in m s^{-1}, with positive velocities as along-channel inflows and negative velocities as along-channel outflows.

Fig. 8. West to east contour plot of density and temperature in Tahsis Inlet from UCTD transect Tu4. Density is reported in sigma theta and temperature reported in Celsius.

Fig. 9. a) West to east contour plot of density in Tahsis Inlet from UCTD transect Tu5. Density is reported in sigma theta. b) Calculated geostrophic velocities against depth for cross-channel UCTD transect Tu5. Velocities are reported in m s^{-1}.

Fig. 10. a) North to south contour plot of density in Muchalat Inlet from UCTD transect Mu1. Density is reported in sigma theta. b) Calculated geostrophic velocities and mean ADCP velocities against depth for cross-channel UCTD transect Mu1. Velocities are reported in m s^{-1}, with positive velocities as along-channel inflows and negative velocities as along-channel outflows.

Fig. 11. a) North to south contour plot of density in Muchalat Inlet from UCTD transect Mu2. Density is reported in sigma theta. b) Calculated geostrophic velocities mean ADCP velocities against depth for cross-channel UCTD transect Mu2. Velocities are reported in m s^{-1}, with positive velocities as along-channel inflows and negative velocities as along-channel outflows.

Fig. 12. a) North to south contour plot of density in Muchalat Inlet from UCTD transect Mu3. Density is reported in sigma theta. b) Calculated geostrophic velocities and mean ADCP velocities against depth for cross-channel UCTD transect Mu3. Velocities are reported in m s^{-1}, with positive velocities as along-channel inflows and negative velocities as along-channel outflows.

Figures

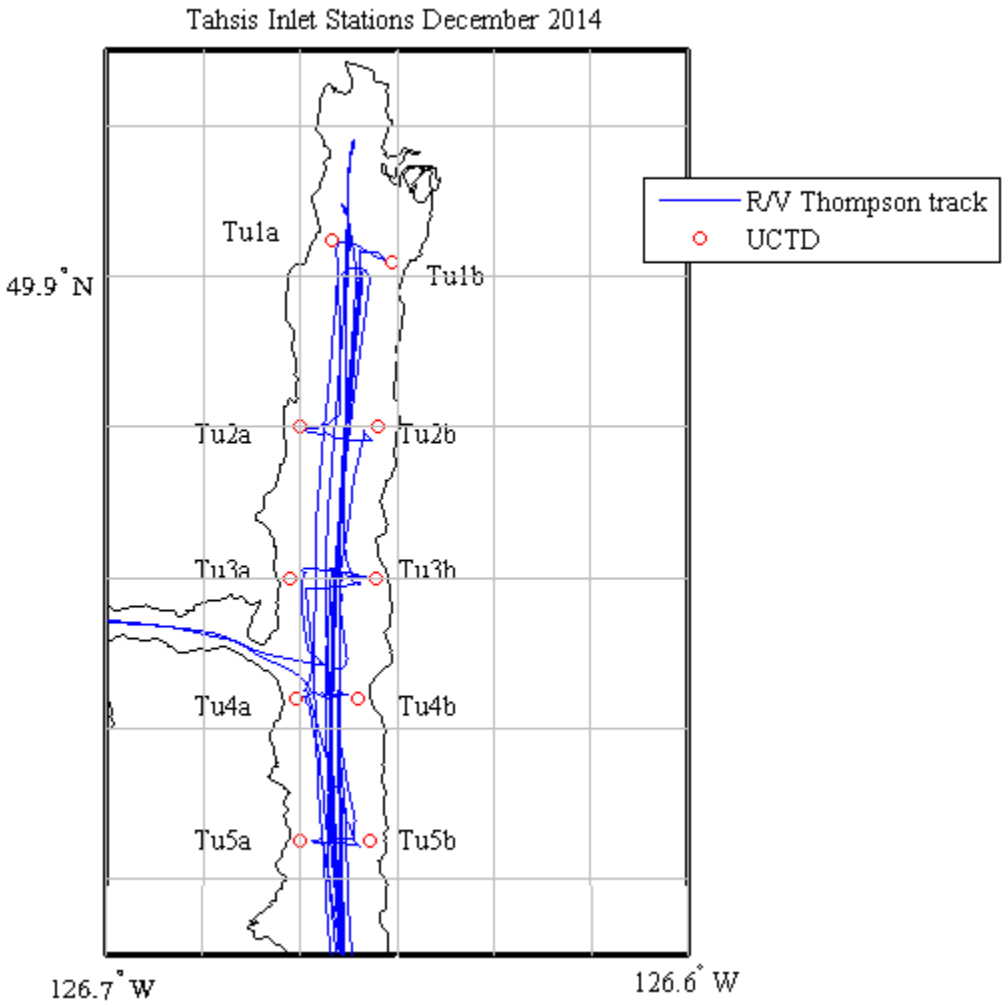

Fig. 1.

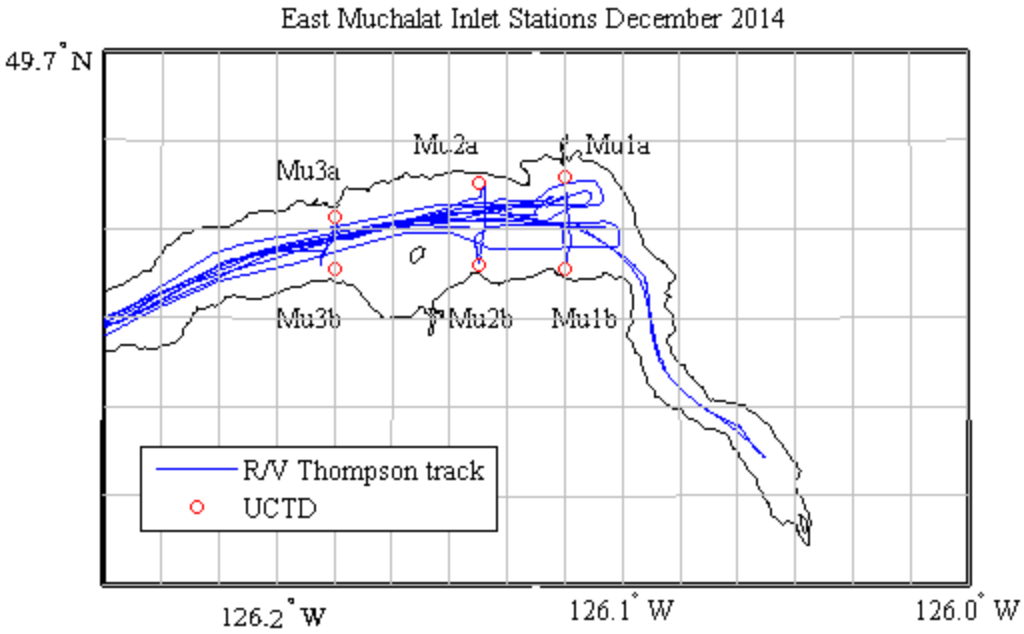
East Muchalat Inlet Stations December 2014
49.7° N
Mu3a
Mu2a
Mu1a
Mu3b
Mu2b
Mu1b
R/V Thompson track
UCTD
126.2° W
126.1° W
126.0° W

Fig. 2.

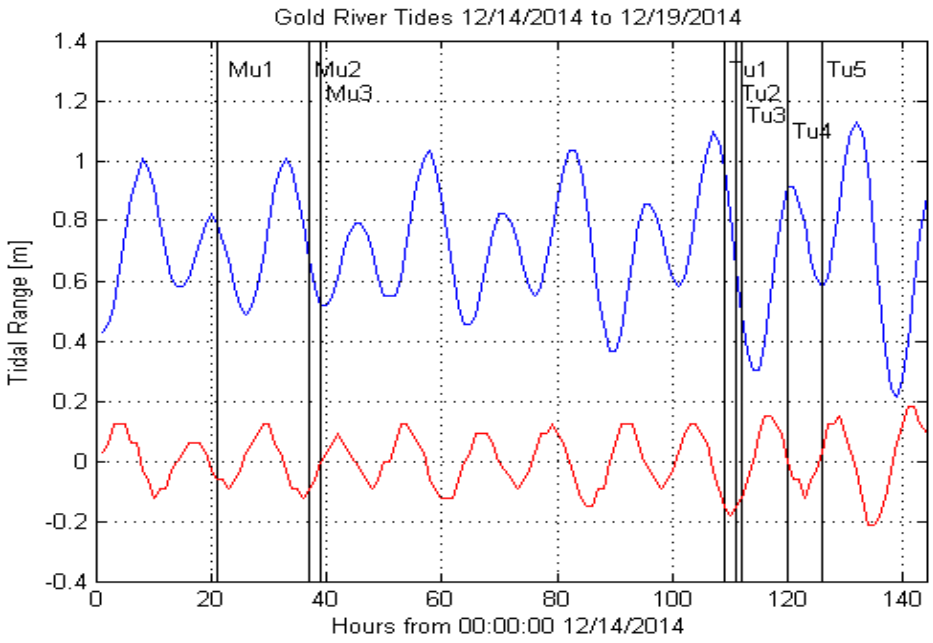
Gold River Tides 12/14/2014 to 12/19/2014
Mu1
Mu2
Mu3
Tu1
Tu2
Tu3
Tu4
Tu5
Tidal Range [m]
Hours from 00:00:00 12/14/2014
1.4
1.2
1
0.8
0.6
0.4
0.2
0
-0.2
-0.4
0
20
40
60
80
100
120
140

Fig. 3.

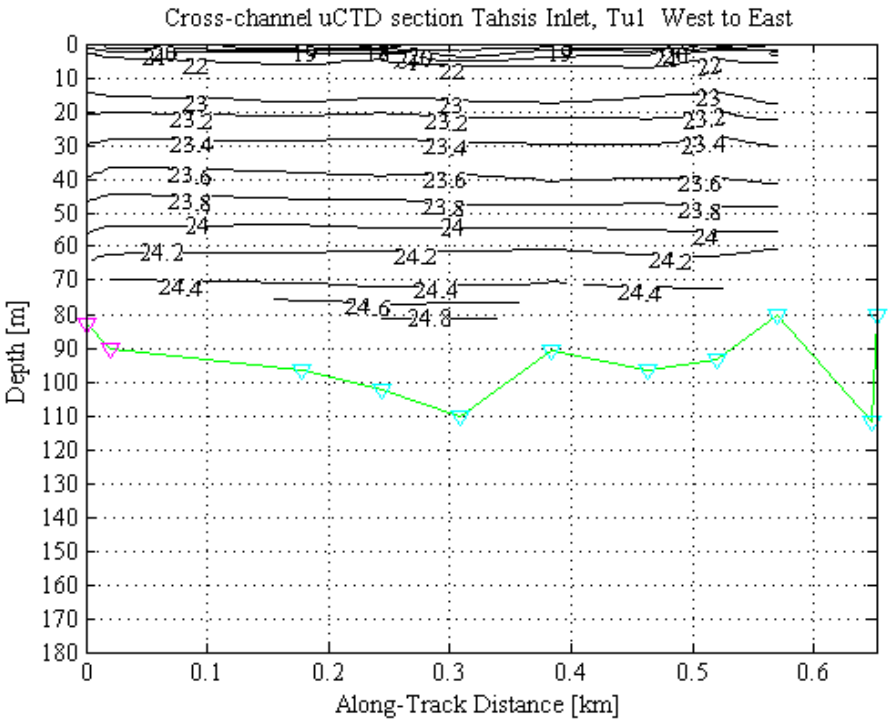
Cross-channel uCTD section Tahsis Inlet, Tu1 West to East
Depth [m]
Along-Track Distance [km]

a)

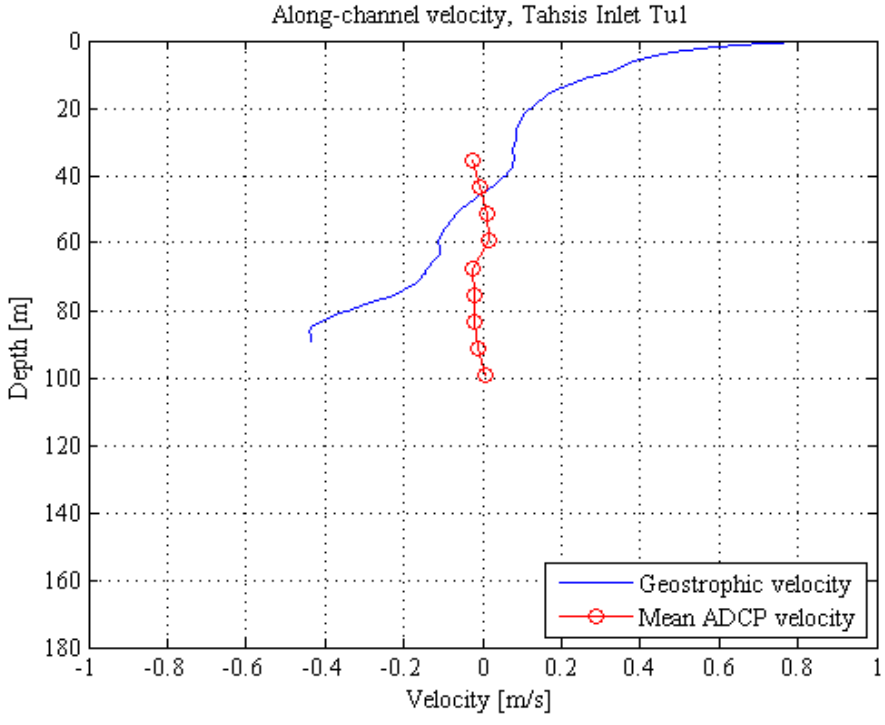
Along-channel velocity, Tahsis Inlet Tu1
Depth [m]
Velocity [m/s]
Geostrophic velocity
Mean ADCP velocity

b)

Fig. 4

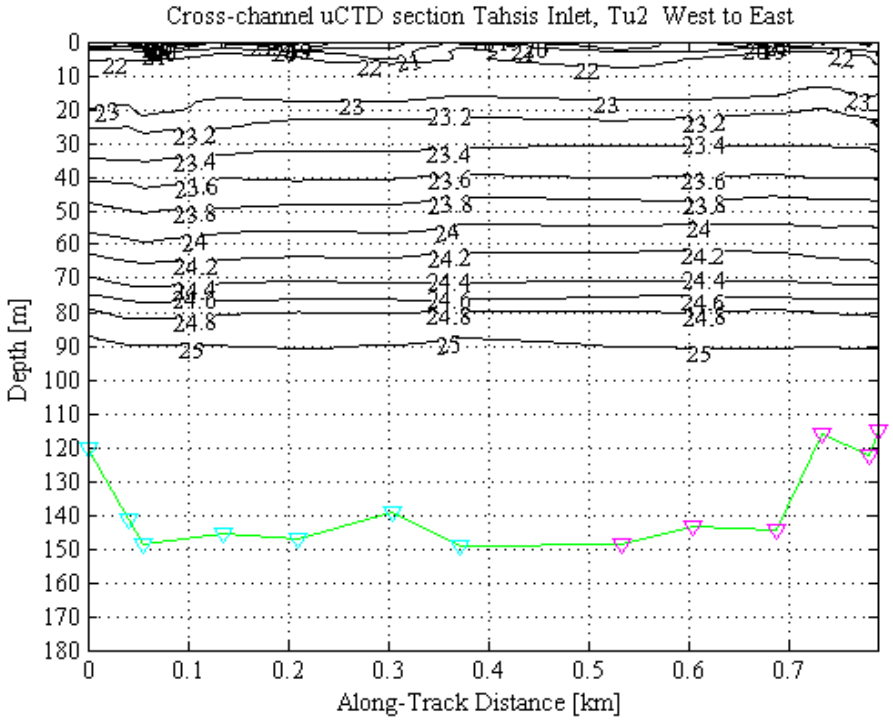
Cross-channel uCTD section Tahsis Inlet, Tu2 West to East
Depth [m]
Along-Track Distance [km]

a).

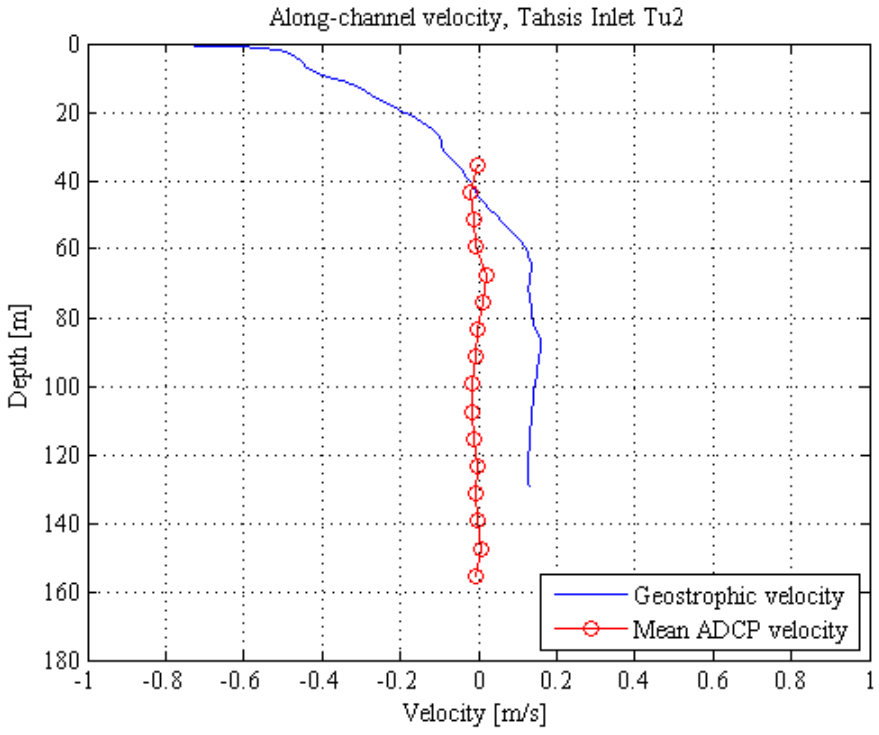
Along-channel velocity, Tahsis Inlet Tu2
Depth [m]
Velocity [m/s]
Geostrophic velocity
Mean ADCP velocity

b)

Fig. 5.

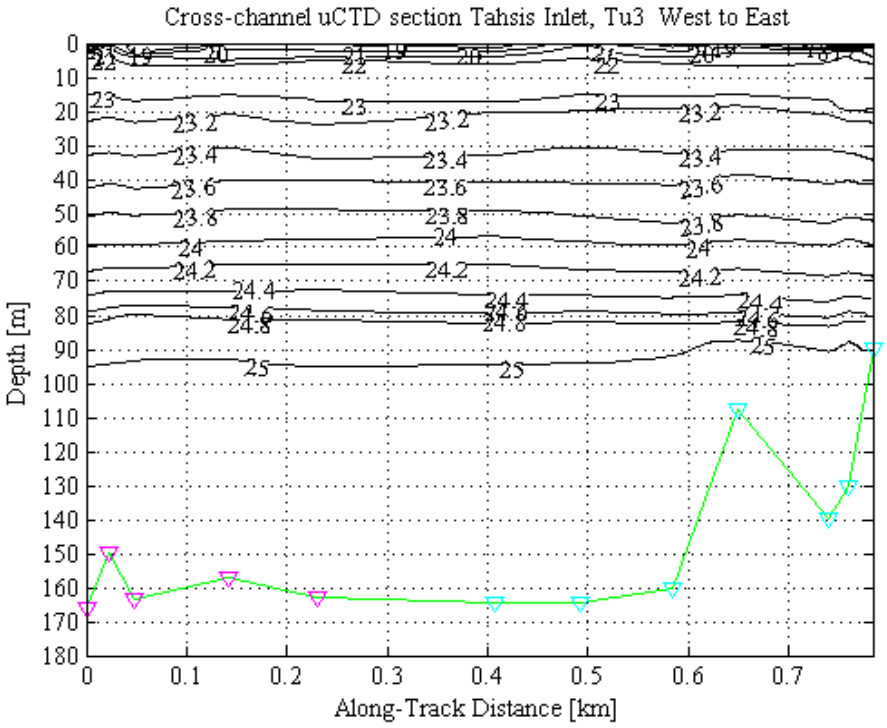
Cross-channel uCTD section Tahsis Inlet, Tu3 West to East
Depth [m]
Along-Track Distance [km]

a)

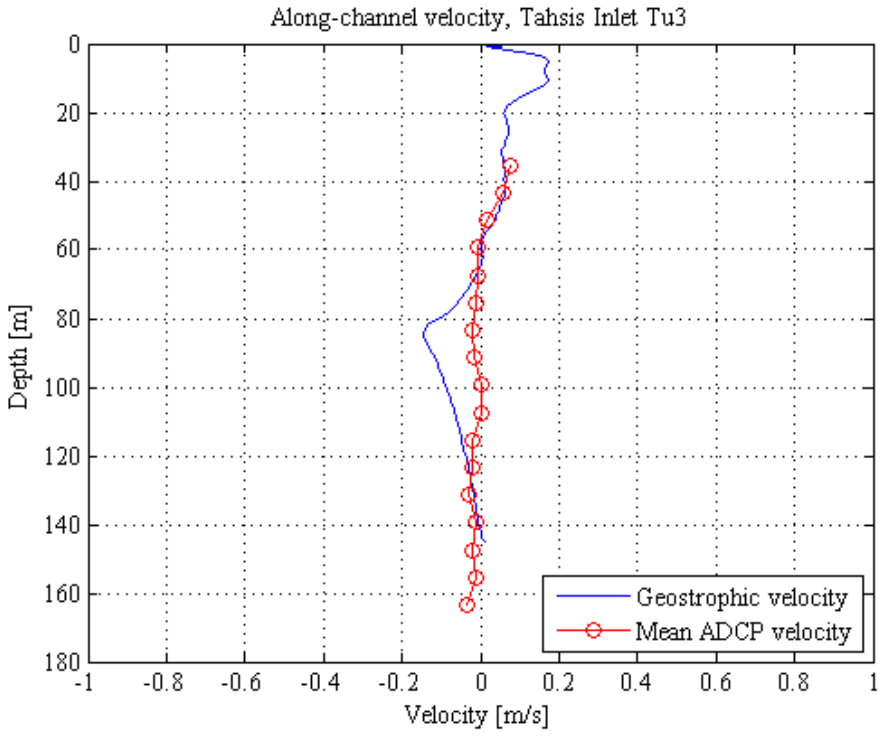
Along-channel velocity, Tahsis Inlet Tu3
Depth [m]
Velocity [m/s]
Geostrophic velocity
Mean ADCP velocity

b)

Fig. 6.

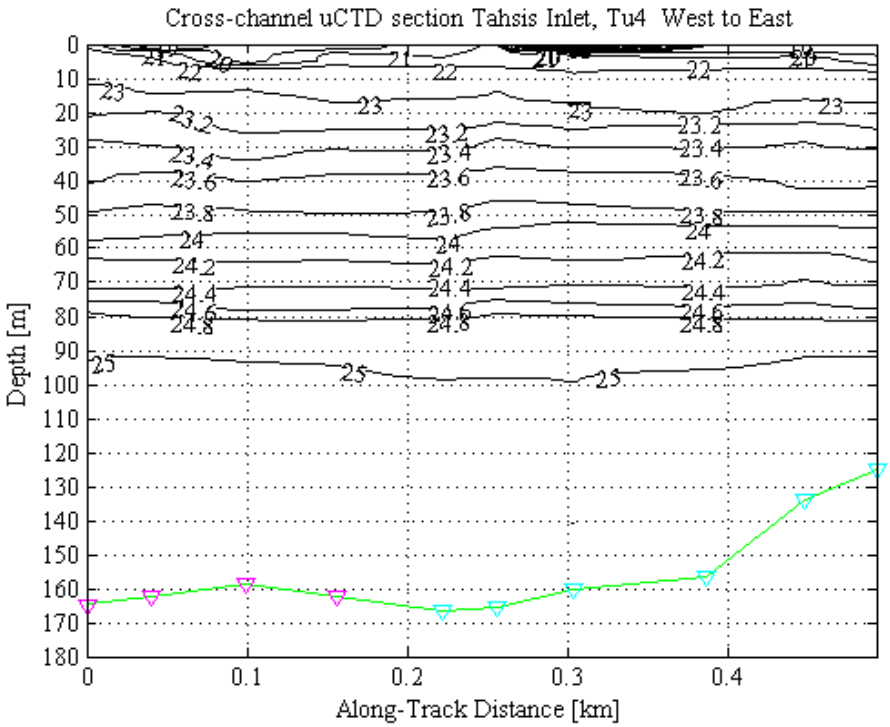
Cross-channel uCTD section Tahsis Inlet, Tu4 West to East
Depth [m]
Along-Track Distance [km]

a)

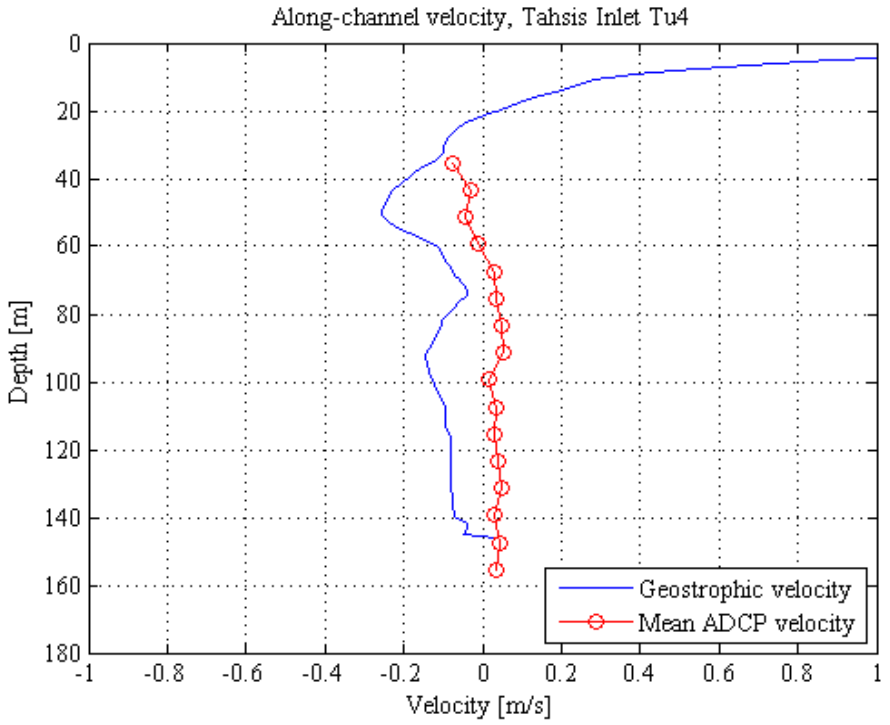
Along-channel velocity, Tahsis Inlet Tu4
Depth [m]
Velocity [m/s]
Geostrophic velocity
Mean ADCP velocity

b)

Fig. 7.

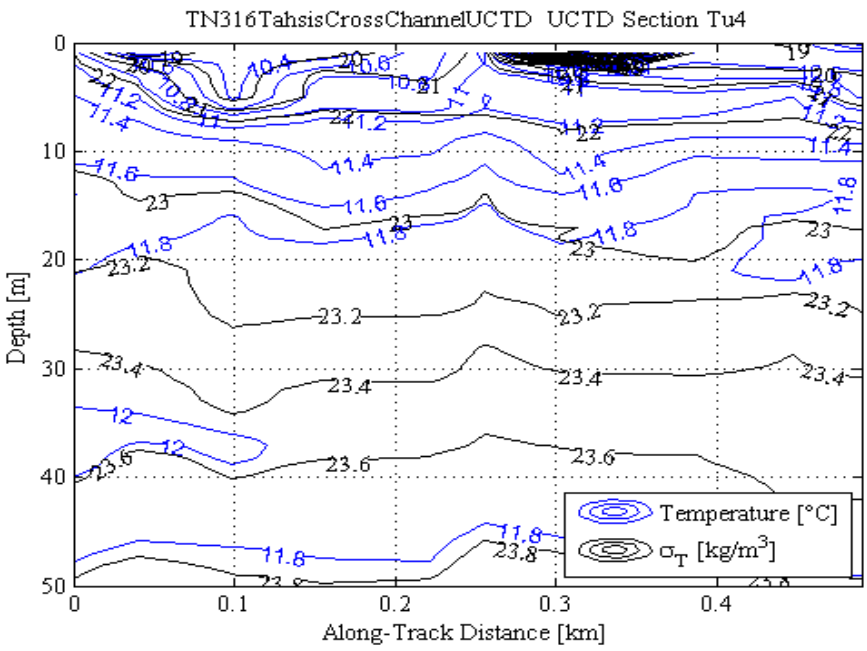
TN316TahsisCrossChannelUCTD UCTD Section Tu4
Depth [m]
Along-Track Distance [km]
Temperature [°C]
σT [kg/m3]

Fig. 8.

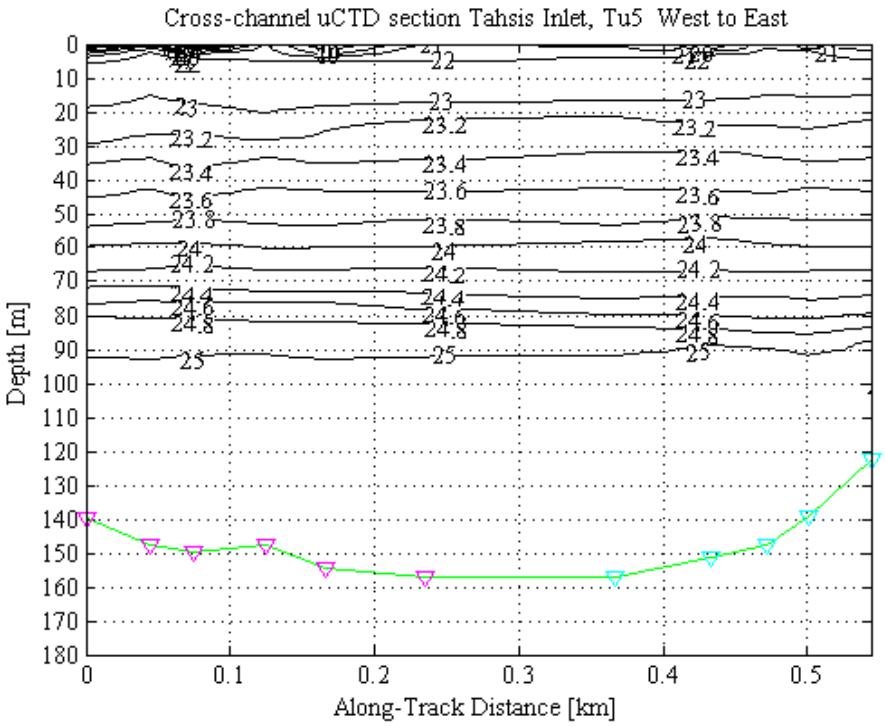
Cross-channel uCTD section Tahsis Inlet, Tu5 West to East
Depth [m]
Along-Track Distance [km]

a)

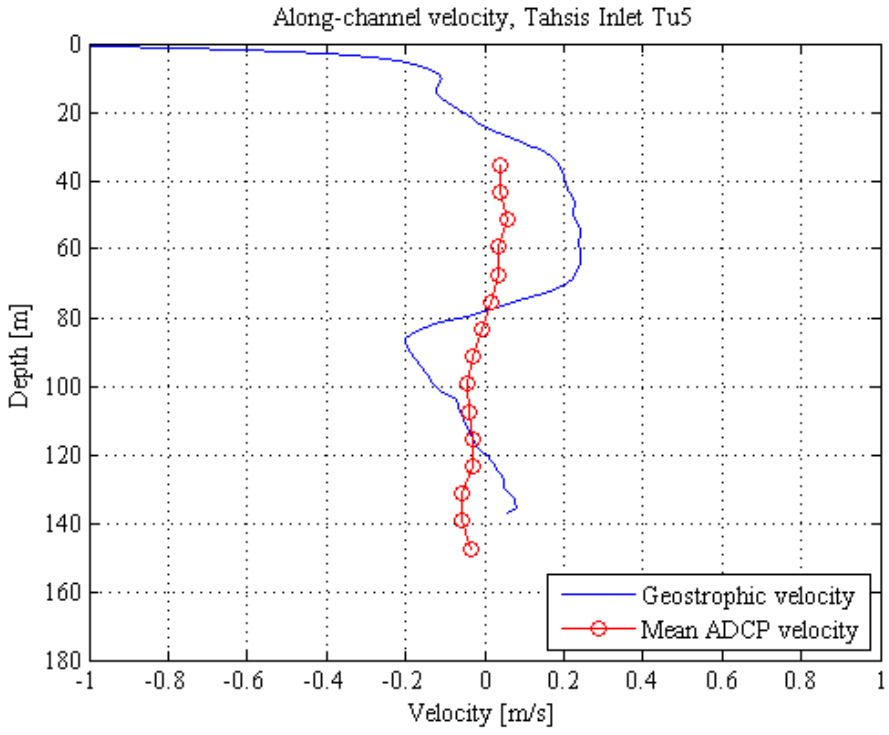
Along-channel velocity, Tahsis Inlet Tu5
Depth [m]
Velocity [m/s]
Geostrophic velocity
Mean ADCP velocity

b)

Fig. 9.

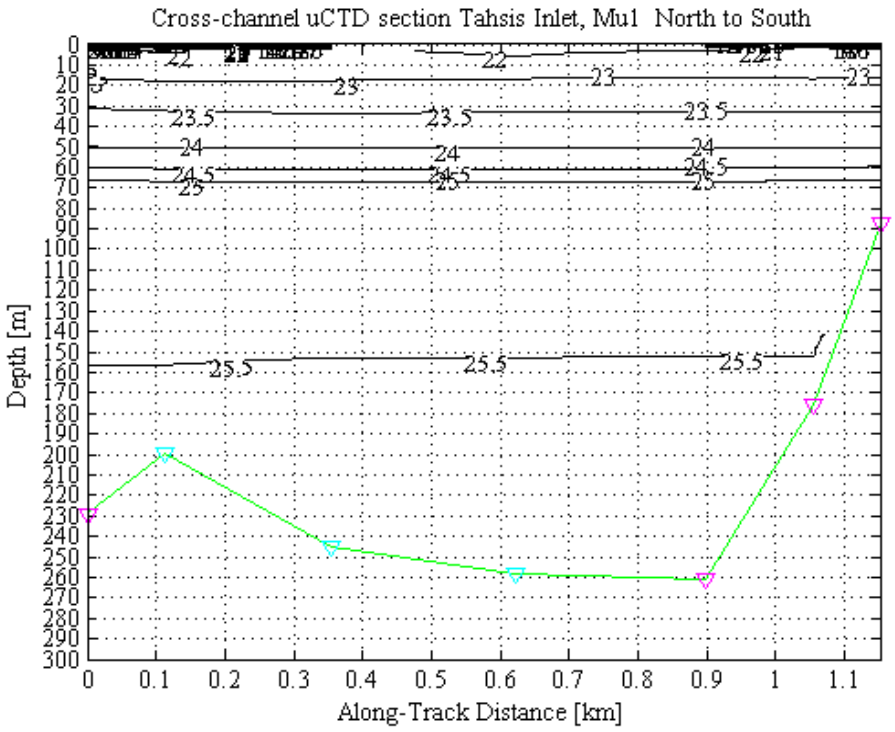
Cross-channel uCTD section Tahsis Inlet, Mu1 North to South
Depth [m]
Along-Track Distance [km]
22
23
23.5
24
24.5
25
25.5

a)

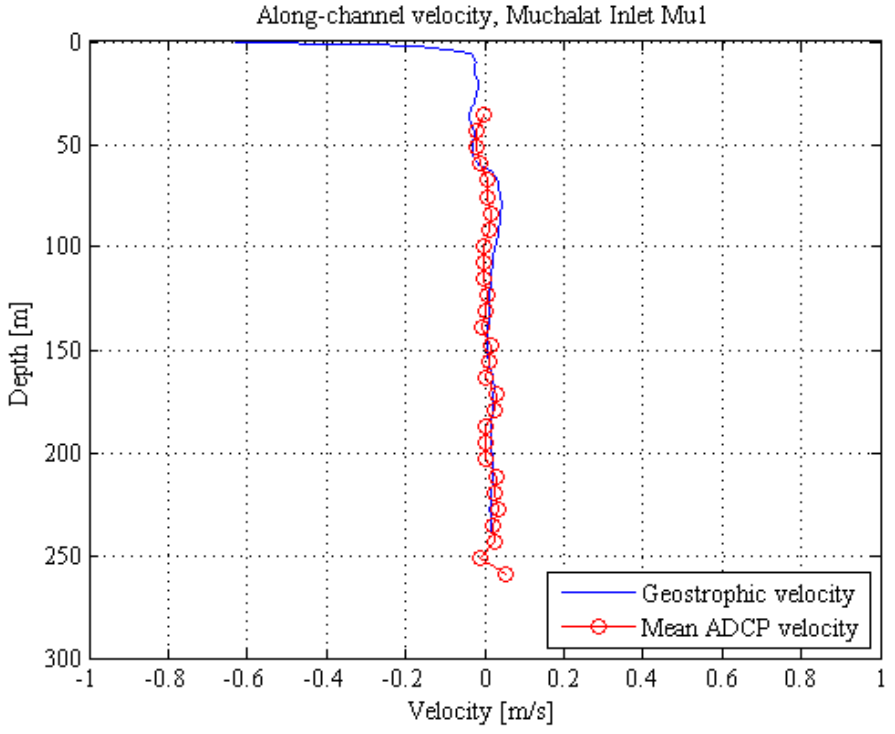
Along-channel velocity, Muchalat Inlet Mu1
Depth [m]
Velocity [m/s]
Geostrophic velocity
Mean ADCP velocity

b)

Fig. 10.

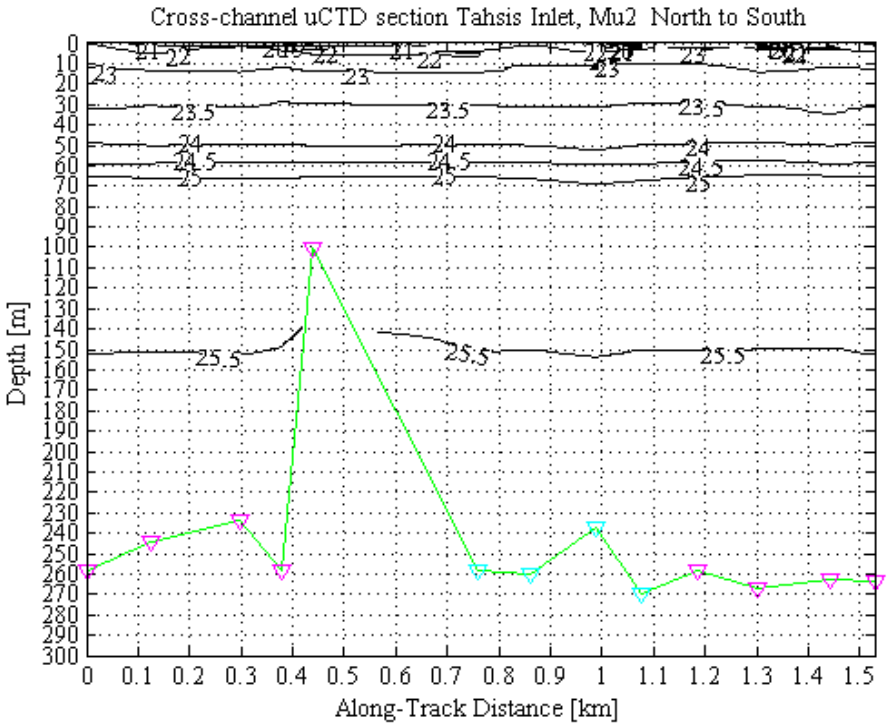
Cross-channel uCTD section Tahsis Inlet, Mu2 North to South
Depth [m]
Along-Track Distance [km]

a)

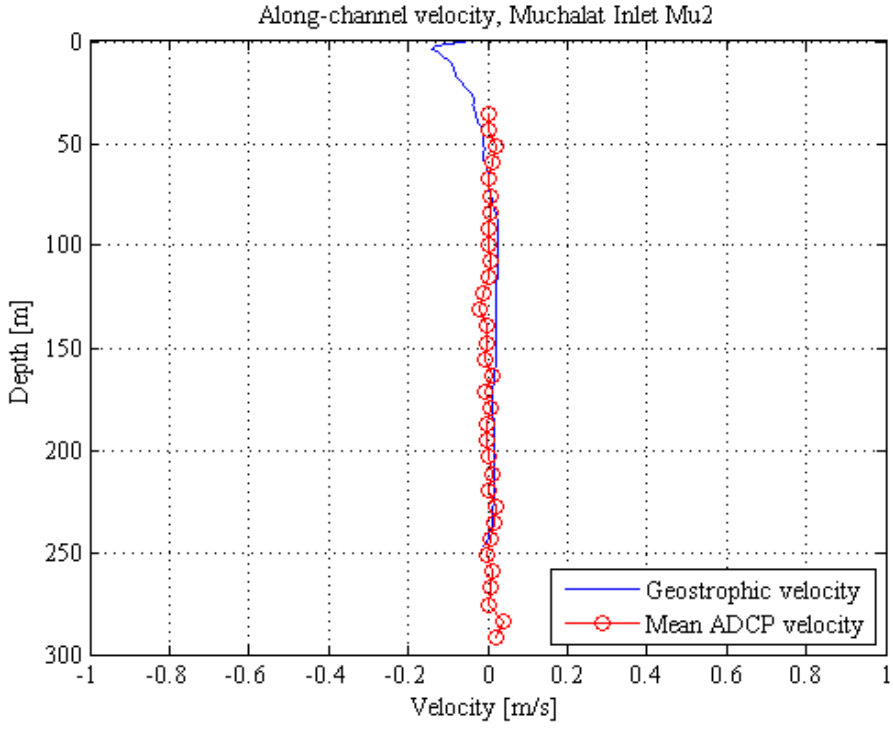
Along-channel velocity, Muchalat Inlet Mu2
Depth [m]
Velocity [m/s]
Geostrophic velocity
Mean ADCP velocity

b)

Fig.11.

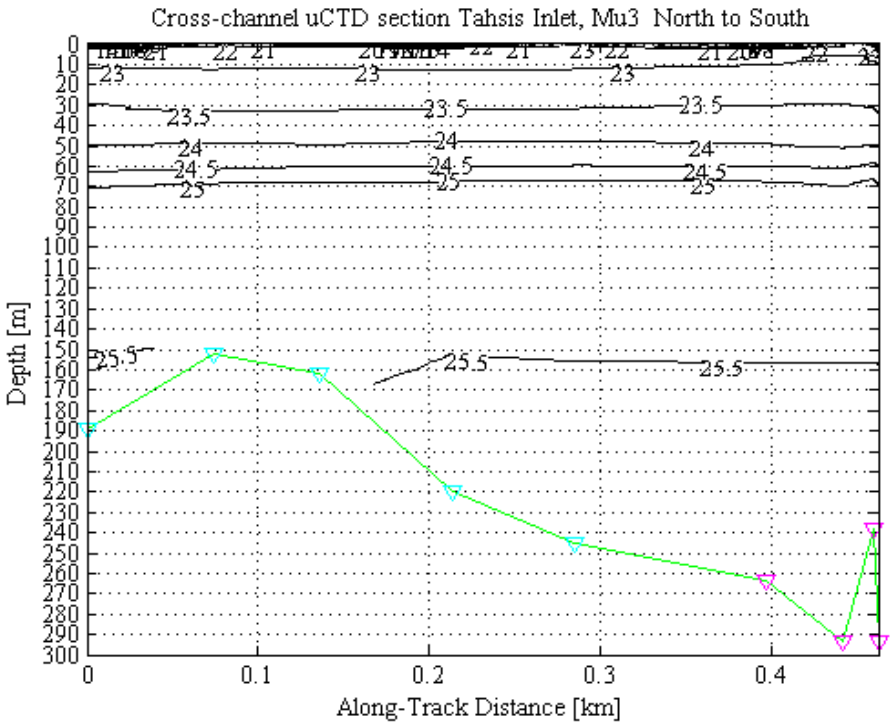
Cross-channel uCTD section Tahsis Inlet, Mu3 North to South
Depth [m]
Along-Track Distance [km]

a)

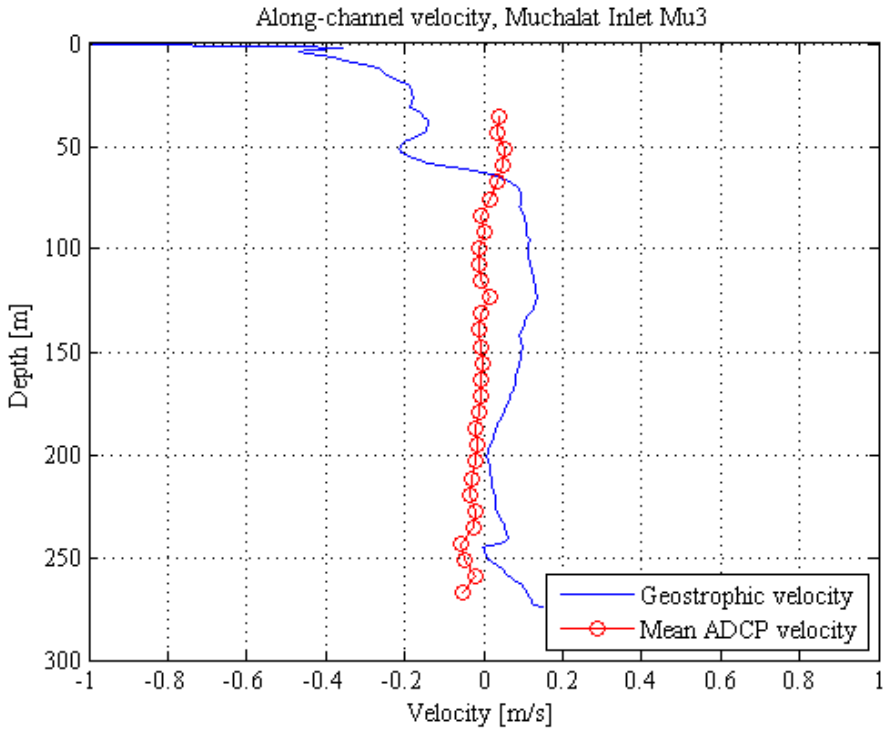
Along-channel velocity, Muchalat Inlet Mu3
Depth [m]
Velocity [m/s]
Geostrophic velocity
Mean ADCP velocity

b)

Fig. 12.

References

Cameron, W. M. 1951. On the transverse forces in a British Columbia inlet. Transactions of the Royal Society of Canada, **45**, 1-9.

Dyer, K. 1997. Estuaries, A Physical Introduction, 2nd ed. Wiley, New York. 1-195.

Farmer, D. M. and H. J. Freeland. 1983. The physical oceanography of fjords. Progress in Oceanography, **12**: 147-219.

Forrester, W. D. 1970. Geostrophic approximation in the St. Lawrence estuary. Tellus, **22**: 53-65.

Gill, A. E. 1982. Atmosphere-ocean dynamics, Vol. 30. Academic press. 198-245.

Jackson, C., B. Cook. 1999. Gold-Tahsis-Zeballos Water Allocation Plan, Province of British Columbia Ministry of Environment Lands and Parks Vancouver Island Region Report. 1-53.

Tabata, S. and G. L. Pickard. 1957. The physical oceanography of Bute inlet, British Columbia. Journal of the Fisheries Board of Canada. **14**: 487-520.

Teledyne Oceanscience. 2014. UnderwayCTD. http://www.oceanscience.com/products/underway-systems/underway-ctd.aspx. 10/31/2014